Structural Study of Various Substituted Biphenyls and Their Radical Anions Based on Time-Resolved Resonance Raman Spectroscopy Combined with Pulse Radiolysis

ARTICLE *in* THE JOURNAL OF PHYSICAL CHEMISTRY A · JANUARY 2015

Impact Factor: 2.69 · DOI: 10.1021/jp511229t · Source: PubMed

THE JOURNAL OF PHYSICAL CHEMISTRY A

Article

pubs.acs.org/JPCA

Structural Study of Various Substituted Biphenyls and Their Radical Anions Based on Time-Resolved Resonance Raman Spectroscopy Combined with Pulse Radiolysis

Jungkweon Choi,*[,†,‡] Dae Won Cho,[§] Sachiko Tojo,[†] Mamoru Fujitsuka,[†] and Tetsuro Majima*[,†]

[†]The Institute of Scientific and Industrial Research (SANKEN), Osaka University, Mihogaoka 8-1, Ibaraki, Osaka 567-0047, Japan

[‡]Center for Nanomaterials and Chemical Reactions, Institute for Basic Science (IBS), Daejeon 305-701, Republic of Korea

[§]Department of Advanced Materials Chemistry, Korea University, Sejong Campus, Sejong 339-700, Korea

Supporting Information

ABSTRACT: The structures of various *para*-substituted biphenyls (Bp-X; X = −OH, $-OCH_3$, $-CH_3$, −H, $-CONH_2$, −COOH, and −CN) and their radical anions ($Bp\text{-}X^{\bullet-}$) were investigated by time-resolved resonance Raman spectroscopy combined with pulse radiolysis. The inter-ring C1−C1′ stretching modes (ν_6) of Bp-X were observed at ∼1285 cm^{-1}, whereas the ν_6 modes of $Bp\text{-}X^{\bullet-}$ with an electron-donating or -withdrawing substituent were significantly up-shifted. The difference (Δf) between the ν_6 frequencies of Bp-X and $Bp\text{-}X^{\bullet-}$ showed a significant dependence on the electron affinity of the substituent and exhibited a correlation with the Hammett substituent constants (σ_p). In contrast to $Bp\text{-}H^{\bullet-}$ with a planar geometry, the theoretical and experimental results reveal that all $Bp\text{-}X^{\bullet-}$ with an electron-donating or -withdrawing substituent have a slightly twisted structure. The twisted structure of $Bp\text{-}X^{\bullet-}$ is due to the localization of the unpaired electron and negative charge density on one phenyl moiety in $Bp\text{-}X^{\bullet-}$.

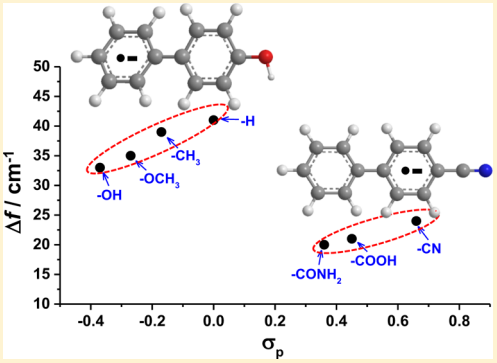

INTRODUCTION

Biphenyl (Bp-H), which consists of two benzene rings with weak electronic interactions, has been experimentally and theoretically investigated to understand its structure in gas, liquid, and solid phases.[1−13] To this end, the steady-state and time-resolved resonance Raman (TR^3) spectroscopic techniques have been extensively used because of their ability to provide useful information regarding the structure and dynamics of short-lived species such as radical ions.[11,13−19] As a result, it is well-known that in the gas and liquid phases, Bp-H has a twisted structure due to steric hindrance between the *ortho* hydrogen atoms, whereas in the solid state Bp-H has a planar structure. In contrast to neutral Bp-H, its radical ions (radical anion $Bp\text{-}H^{\bullet-}$ and radical cation $Bp\text{-}H^{\bullet+}$) tend to have a quinoidal character, resulting in a planar structure even in the liquid phase.

However, there are a number of arguments for the structure of $Bp\text{-}H^{\bullet-}$ and $Bp\text{-}H^{\bullet+}$ in solution. For instance, the theoretical and experimental results of Lapouge et al. revealed that $Bp\text{-}H^{\bullet-}$ has a planar structure, whereas $Bp\text{-}H^{\bullet+}$ has a slightly twisted structure.[13] Furthermore, most studies have been focused on halogen-substituted biphenyls, because of the pollution concerns related to polychlorinated biphenyls (PCB). Mönig et al. suggested that the radical cations of PCB in dichloroethane (DCE) have either a planar or a twisted structure and that the population of the two conformers depends on the number of chlorine atoms at the *ortho* position to the pivot bond.[9] Therefore, only a few studies have been conducted on biphenyls substituted asymmetrically with electron-donating or -withdrawing substituents.

Here, we present the comparative investigation of the structures of Bp-X and $Bp\text{-}X^{\bullet-}$ with electron-donating or -withdrawing substituents at the *para* position (Scheme 1) using TR^3 spectroscopic measurements combined with pulse radiolysis. Theoretical calculations for the structures of Bp-X and $Bp\text{-}X^{\bullet-}$ are also conducted and compared to the experimental results. Pulse radiolysis can easily generate radical ions by irradiation with high-energy electrons.[9,20−22] Thus, pulse radiolysis has been extensively used to study transient

Scheme 1. Structures of Biphenyls with Various Substituents at *para*-Position (Bp-X)

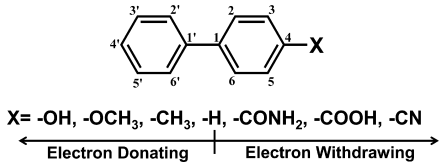

Received: November 10, 2014
Revised: December 20, 2014
Published: January 10, 2015

DOI: 10.1021/jp511229t
J. Phys. Chem. A 2015, 119, 851−856

radical species during the redox reactions of various molecules.[20−23]

On the other hand, the photoionization technique is a well-known method for generating radical cations of molecules having low ionization potentials.[9,20,22,24] In addition, other techniques using the chemical redox and electrochemical reaction are also popular methods for the generation of radical ions. Nevertheless, pulse radiolysis is a unique tool that can generate radical cations or anions selectively and efficiently, allowing us to study its properties, including its reactivity.[25−28] Usually, pulse radiolysis is combined with the transient absorption spectroscopic technique to investigate the electronic structures of radical species. However, we have attempted to combine TR^3 spectroscopy with pulse radiolysis to understand the molecular structures, based on the vibrational levels, of transient species, such as reaction intermediates and radical ions, generated by pulse radiolysis.[22,23,29] The results presented herein clearly show that the structure of Bp-$X^{\bullet-}$ is significantly affected by the electron affinity of the substituent, while the structure of Bp-X depends predominantly on the steric hindrance between the *ortho* hydrogen atoms. The difference (Δf) between the frequencies of the C_1-C_1' (ν_6 mode) of Bp-X and Bp-$X^{\bullet-}$ shows a correlation with the Hammett substituent constants (σ_p). In this Article, we will discuss the structural changes of Bp-X and Bp-$X^{\bullet-}$, as well as the correlation between the σ_p and Δf values.

RESULTS AND DISCUSSION

Figure 1 shows the transient absorption spectra measured during pulse radiolysis of Bp-H, Bp-OH, and Bp-CN generated

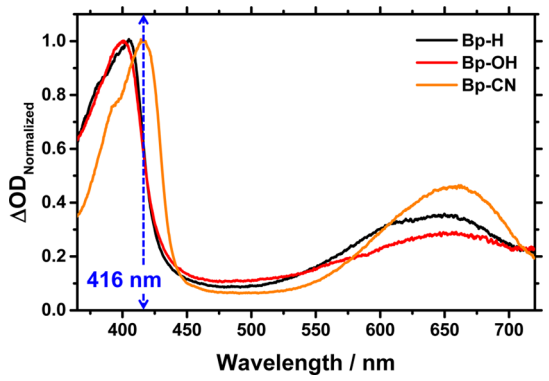

Figure 1. Transient absorption spectra measured with a delay of 50 ns after the electron pulse during the pulse radiolysis of Bp-H, Bp-OH, and Bp-CN in DMF. Transient absorption spectra of other Bp-X's are shown in SI Figure S1.

by pulse radiolysis in dimethylformamide (DMF) solutions. The transient absorption spectra of other Bp-X's are shown in Supporting Information (SI) Figure S1. For Bp-H, the transient absorption bands observed at ∼400 and ∼650 nm can be assigned to Bp-$H^{\bullet-}$ on comparing with the previously reported results.[18,24,30] Other Bp-Xs exhibit similar transient absorption spectral features, consisting of two strong absorption bands at ∼400 and ∼650 nm as shown in Figure 1 and SI Figure S1. Therefore, the two absorption bands at ∼400 and ∼650 nm for other Bp-X's are easily assigned to the Bp-$X^{\bullet-}$ generated by pulse radiolysis in DMF. This is because the solvated electron (e_{sol}^-), generated from DMF by pulse radiolysis, reacts with Bp-X quickly, resulting in the formation of Bp-$X^{\bullet-}$ according to the following reactions:

$$\text{DMF} \rightsquigarrow \text{DMF}^{\bullet+} + e_{sol}^-$$

$$\text{Bp-X} + e_{sol}^- \rightarrow \text{Bp-X}^{\bullet-}$$

Buntinx and Poizat suggested that the Bp-$H^{\bullet+}$ → Bp-$H^{\bullet+}$* absorption at ∼400 nm corresponds to the HOMO (ϕ_6) → LUMO (ϕ_7) transition, which leads to the reinforcement of the quinoidal distortion, and thus the $\phi_6 \rightarrow \phi_7$ transition can be distributed over the entire configuration of Bp-$H^{\bullet+}$ more uniformly.[18] Therefore, to investigate the substituent effect on the structures of Bp-X and Bp-$X^{\bullet-}$, we measured their TR^3 spectra during pulse radiolysis in DMF. The 416 nm laser pulse, generated by hydrogen Raman shifting of the third harmonic (355 nm) from a nanosecond Q-switched Nd:YAG laser, was used to measure the TR^3 spectra of Bp-$X^{\bullet-}$ at the resonance wavelength (Figure 1).

Figure 2 and SI Figure S2 show the Raman spectra of Bp-X and Bp-$X^{\bullet-}$ in DMF. The TR^3 spectra of Bp-$X^{\bullet-}$ were

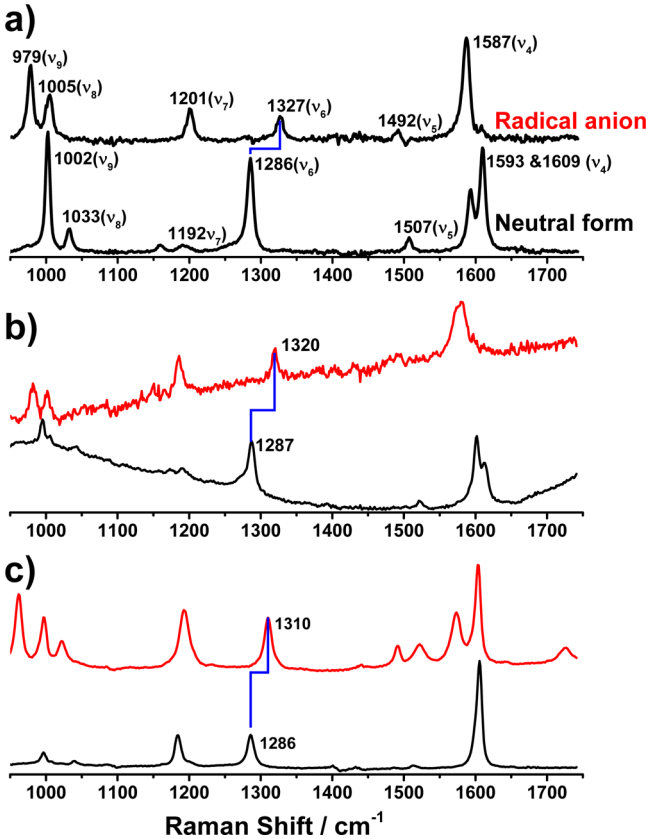

Figure 2. TR^3 spectra of Bp-X (black line) and Bp-$X^{\bullet-}$ (red line) in DMF; Bp-H (a), Bp-OH (b), and Bp-CN (c). TR^3 spectra of Bp-$X^{\bullet-}$ were measured with a delay of 50 ns after the radiation of electron pulse during the pulse radiolysis of Bp-H, Bp-OH, and Bp-CN in DMF. TR^3 spectra of other Bp-X's are shown in SI Figure S2.

measured with a delay of 50 ns after the electron pulse irradiation by pulse radiolysis in DMF. The Raman spectra of Bp-$X^{\bullet-}$, shown in Figure 2 and SI Figure S2, are significantly different from those of Bp-X. On the basis of previously reported spectra for Bp-H and Bp-$H^{\bullet-}$,[11,13,19,30] the Raman modes for Bp-X and Bp-$X^{\bullet-}$, listed in Table 1, can be assigned easily. In the present study, we focused on the inter-ring C_1-

DOI: 10.1021/jp511229t
J. Phys. Chem. A 2015, 119, 851−856

Table 1. Observed Raman Bands of Bp-X and Bp-X$^{\bullet-}$ in DMF[a]

	−OH	−OCH_3	−CH_3	−H	−$CONH_2$	−COOH	−CN
C═O					(1660)	1668	
ν_4	1613 (1581) 1602	1608 (1587) 1602	1614 (1587) 1602	1610 (1587) 1593	1609 (1607) 1600 (1582)	1609 (1618) 1602 (1566)	1606 (1604) (1573)
ν_5	1520 (1493)	1501 (1496)	1520 (1498)	1507 (1492)	– (1491)	1502 (1492)	1513 (1492) (1522)
ν_6	1287 (1320)	1288 (1323)	1287 (1326)	1286 (1327)	1287 (1307)	1287 (1308)	1286 (1310)
ν_7	1190 (1186)	1190 (1193)	1196 (1193) 1160?	1191 (1201)	1199 (1208) (1172)	1194 (1197)	1185 (1193)
ν_8	1043 (1002)	1032 (1002)	1040 (1004)	1032 (1005)	1040 (1023)	1040 (1026)	1039 (1022)
ν_9	1006 (982) 995	1003 (979) 995	1007 (983) 995	1003 (979)	1006 (999) 995? (963)	1008 (999) 996? (966)	1006 (996) 996? (962)

[a]The values in parentheses are the frequencies for Bp-X$^{\bullet-}$ in DMF. ν_4: Phenyl C═C stretching motions and phenyl C−C−H bending. ν_5: Phenyl C═C stretching motions. ν_6: Inter-ring C−C stretching. ν_7: Phenyl C−C−H bending motions and CH in-plane bends. ν_8: CH in-plane bends. ν_9: Ring deformation.

Table 2. Structural Parameters of Bp-X and Bp-X$^{\bullet-}$, and the Difference (Δf) between Frequencies (f) of ν_6 for Bp-X and Bp-X$^{\bullet-}$[a]

		X						
		−OH	−OCH_3	−CH_3	−H	−$CONH_2$	−COOH	−CN
σ_p		−0.37	−0.27	−0.17	0	0.36	0.45	0.66
$r_{C1-C1'}$ (Å)	Bp-X	1.484	1.484	1.485	1.486	1.484	1.484	1.484
	Bp-X$^{\bullet-}$	1.439	1.439	1.439	1.439	1.448	1.448	1.444
D (deg)	Bp-X	40.22	40.03	40.57	41.08	40.35	39.94	40.14
	Bp-X$^{\bullet-}$	4.24	2.37	0.16	0	9.16	8.96	0.01
f (cm^{-1})	Bp-X	1287	1288	1287	1286	1287	1287	1286
	Bp-X$^{\bullet-}$	1320	1323	1326	1327	1307	1308	1310
	Δf	33	35	39	41	20	21	24

[a]The $r_{C1-C1'}$ and D values are calculated at B3LYP/6-311+G(d,p). r: Distance between the inter-ring C1−C1′ bond. D: Dihedral angle around the inter-ring C1−C1′ bond. f: Frequency of ν_6 corresponding to the inter-ring C1−C1′ stretch. Δf: $f_{Bp\text{-}X} - f_{Bp\text{-}X^{\bullet-}}$.

C_1' stretching modes (ν_6) to obtain information regarding the structural changes of Bp-X and Bp-X$^{\bullet-}$.

The ν_6 modes for Bp-H and Bp-H$^{\bullet-}$, observed at 1286 and 1327 cm^{-1}, respectively (Figure 2a), are consistent with those reported by previous studies. Notably, the ν_6 modes for Bp-X's are observed at 1286−8 cm^{-1}, which are close to that of Bp-H. These results imply that the structures of Bp-X's are not affected by the substituents attached at the *para* position (C_4) of the phenyl ring. Bp-H has a twisted structure in the liquid phase because of the repulsion of the *ortho* hydrogens. Because the ν_6 modes of Bp-H and Bp-X's are observed at similar frequencies (1286−8 cm^{-1}), it can be expected that the other Bp-X's also have a twisted structure with respect to the two benzene rings. This result for Bp-X indicates that the presence of substituents at the *para* position has no effect on the structure of Bp-X, implying that the torsional angle (D) and the bond length ($r_{C1-C1'}$) between the two benzene rings are independent of the electronic properties, such as electron affinity, of the substituents.

The D and $r_{C1-C1'}$ values of the C_1-C_1' linkage between the two benzene rings, for neutral Bp-X, were calculated at the B3LYP/6-311+G(d,p) level. The D and $r_{C1-C1'}$ values for Bp-H calculated at the B3LYP/6-311+G(d,p) level were determined to be 41.08° and 1.486 Å, respectively, as listed in Table 2, and those for other Bp-X's were 40.2 ± 0.3° and 1.484 Å, respectively. Although the electron-donating or -withdrawing groups were introduced as *para* substitutions, the calculated D and $r_{C1-C1'}$ values showed little change. This result supports the hypothesis that the twisted structure is attributable to the repulsion of the *ortho* hydrogens, and not the electronic properties of the *para* substituents.

On the other hand, the ν_6 mode of Bp-X$^{\bullet-}$, shown in Figure 2 and SI Figure S2, is markedly up-shifted. The upshift of the ν_6 mode accompanied by the one-electron reduction has been interpreted in terms of the structural change from Bp-X to Bp-X$^{\bullet-}$ with a quinoidal character. The difference (Δf) between the frequencies of the ν_6 mode for neutral Bp-X and anionic Bp-X$^{\bullet-}$ can be considered an indicator of the change in the bond strength of the central C_1-C_1' bond located between the two benzene rings. Interestingly, the largest Δf, shown in Table 2, was observed for Bp-H. Numerous experimental and theoretical results indicate that Bp-H$^{\bullet-}$ has a shorter $r_{C1-C1'}$ than Bp-H, and that it has a planar structure due to the quinoidal character ($D_{Bp\text{-}H^{\bullet-}}$ = ∼0°).[11,13,14,19,30] Meanwhile, the Δf values for other Bp-X's are smaller than that of Bp-H. This may be attributed to the weak quinoidal character of Bp-X$^{\bullet-}$ as compared to that of Bp-H$^{\bullet-}$, due to the presence of electron-donating or -withdrawing substituents. The smaller Δf values, as compared to Bp-H$^{\bullet-}$, indicate that Bp-X$^{\bullet-}$ may have a slightly twisted structure. To confirm the twisted structure of Bp-X$^{\bullet-}$ with an electron-donating or -withdrawing substituent, their D and $r_{C1-C1'}$ values were calculated at the B3LYP/6-311+G(d,p) level. The theoretical calculations show that the D values of Bp-X$^{\bullet-}$ with an electron-donating or -withdrawing substituent are larger than the 0° observed for Bp-H$^{\bullet-}$, and that their $r_{C1-C1'}$ values are shorter than that of Bp-H$^{\bullet-}$ (1.486 Å) (Table 2). This result supports the hypothesis that the substitution of Bp-H with an electron-donating or -withdrawing group at the *para* position can greatly affect the geometry of Bp-X$^{\bullet-}$, but not of Bp-X.

To further elucidate how the electron affinities of the substituents affect the structure of Bp-X$^{\bullet-}$, we surveyed the

DOI: 10.1021/jp511229t
J. Phys. Chem. A 2015, 119, 851−856

correlation between the observed Δf values and the Hammett substituent constants (σ_p). The Hammett substituent constants were developed and have been substantially used for elucidating the reactivity at an atom directly bonded to a *meta- or para*-substituted aromatic group.[31−33] Furthermore, the Hammett substituent constants are extensively utilized for describing the movement of electrons via the σ- and π-framework. Figure 3

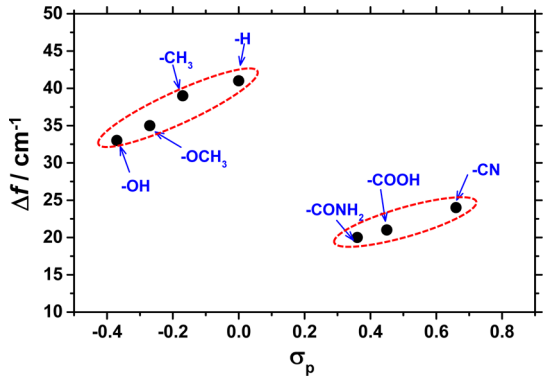

Figure 3. Plots of the frequency difference (Δf) against Hammett σ_p constants for Bp-X's. The frequency difference is $\Delta f = f_{\text{Bp-X}} - f_{\text{Bp-X}^{\bullet-}}$.

shows the plot of the Δf values against the Hammett substituent constants (σ_p) for the different Bp-X substituents. The Δf values reveal the difference between the substituents depending on their electron affinity, either withdrawing or donating; that is, the Δf value decreases on increasing the negative σ_p value of an electron-donating group, while it increases on increasing the positive σ_p value of an electron-withdrawing group. These results suggest that the D and $r_{C1-C1'}$ values for Bp-$X^{\bullet-}$ significantly depend on the electron affinity of the substituent. Indeed, this suggestion is supported by theoretical calculations at the B3LYP/6-311+G(d,p) level. Although the accuracy of theoretical calculations for Bp-$X^{\bullet-}$ and Bp-$X^{\bullet+}$ is still a matter of debate, their results show that the D values of Bp-$X^{\bullet-}$ substituted with an electron-donating or -withdrawing group are larger than those of Bp-$H^{\bullet-}$. On the other hand, the $r_{C1-C1'}$ values of Bp-$X^{\bullet-}$ substituted with an electron-withdrawing group are larger than those of the planar Bp-$H^{\bullet-}$, whereas Bp-$X^{\bullet-}$ with an electron-donating group has $r_{C1-C1'}$ values similar to those of Bp-$H^{\bullet-}$. As depicted in Figure 3, electron-withdrawing groups on Bp-X induce smaller Δf values than do electron-donating groups. These theoretical and experimental results suggest that the quinoidal character of Bp-$X^{\bullet-}$ is weakened upon *para*-substitution with an electron-donating or -withdrawing group, and consequently the planarity of Bp-$X^{\bullet-}$ is lost upon substitution with an electron-donating or -withdrawing group. Indeed, the result presented herein clearly shows that the planarity of Bp-$X^{\bullet-}$ is more greatly affected by an electron-withdrawing group than an electron-donating group.

Here, we further consider the correlation between the Δf values and Hammett substituent constants (σ_p). The opposite effect of electron-donating and -withdrawing substituents on the Δf values, shown in Figure 3, can be interpreted by considering the different distributions of the unpaired electron and negative charge densities of the two benzene rings in Bp-

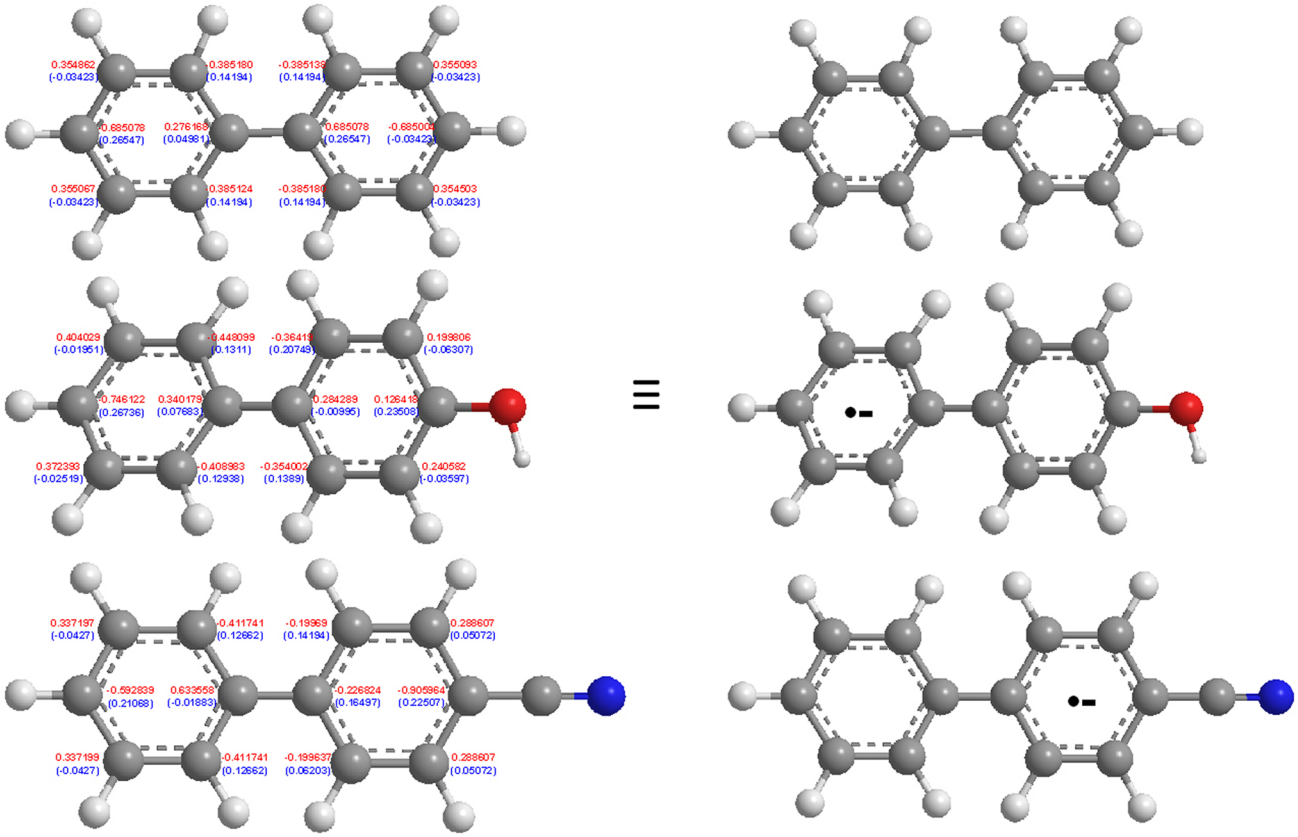

Figure 4. Distribution of the spin (blue) and charge (red) densities in radical anions of Bp-H (top), Bp-OH (middle), and Bp-CN (bottom) calculated at the B3LYP/6-311+G(d,p) level.

DOI: 10.1021/jp511229t
J. Phys. Chem. A 2015, 119, 851−856

$X^{\bullet-}$. To date, it is well-known that the planarity of Bp-$H^{\bullet-}$ is predominantly due to the π-electron delocalization, which results in an increase in the quinoidal character of the two benzene rings; that is, the delocalizations of the unpaired electron and charge densities of the two benzene rings in Bp-$H^{\bullet-}$ are equal. However, the substitution of the *para*-hydrogen atom with an electron-donating or -withdrawing group should result in unequal negative charge densities on the two benzene rings, even in the ground state. In other words, substitution of the *para*-hydrogen atom with an electron-donating group, such as a methyl, methoxy, or hydroxyl group, should increase the negative charge density on the substituted benzene ring, while substitution by an electron-withdrawing group, such as an amide, carboxylic acid, or cyano group, should decrease it. In addition, Mönig et al. suggested that the radical cations of PCBs in DCE show a twisted structure, wherein the unpaired electron and the positive charge are localized mainly on one benzene ring.[9] Taking into account the σ_p-dependence of the Δf values of Bp-X, observed in the present study, and the twisted structure of Bp-$X^{\bullet-}$, we conclude that the unpaired electron and negative charge in Bp-$X^{\bullet-}$ substituted with an electron-donating or -withdrawing group may be localized on one benzene ring with or without a substituent. Consequently, the localization of the unpaired electron and negative charge during pulse radiolysis decreases the quinoidal character of Bp-$X^{\bullet-}$. In this respect, it is important to understand the position of localization of the unpaired electron and negative charge in Bp-$X^{\bullet-}$. Interestingly, theoretical calculations show that in the case of Bp-$X^{\bullet-}$ with an electron-donating group, the sum of the spin and charge density for the unsubstituted benzene ring is larger than that for the substituted benzene ring. However, in the case of Bp-$X^{\bullet-}$ with an electron-withdrawing group, the sum of the spin and charge density for the unsubstituted benzene ring is smaller than that for the substituted benzene ring (Figure 4). This result indicates that the unpaired electron and negative charge density in Bp-$X^{\bullet-}$ substituted with an electron-donating group is located predominantly on the unsubstituted benzene ring, whereas that in Bp-$X^{\bullet-}$ substituted with an electron-withdrawing group is located predominantly on the substituted benzene ring. This result supports the hypothesis that the position of the unpaired electron and negative charge in Bp-$X^{\bullet-}$ significantly depends on the electron affinity of the substituent. These experimental and theoretical results imply that the twisted structure of Bp-$X^{\bullet-}$ is due to the localization of the unpaired electron and negative charge on one benzene ring and that the opposite effect caused by electron-donating and -withdrawing groups on the Δf value stems from the unequal distribution of the spin and charge densities between the two benzene rings in Bp-$X^{\bullet-}$. Therefore, we suggest that the structure of Bp-$X^{\bullet-}$ is predominantly governed by the distribution of the unpaired electron and charge density between the two benzene rings, whereas in the ground state, the structure of Bp-X is governed by the steric interactions between the *ortho* atoms.

CONCLUSION

We have investigated the structures of Bp-X and Bp-$X^{\bullet-}$ using TR^3 spectroscopy combined with pulse radiolysis. The structure of Bp-$X^{\bullet-}$ is significantly affected by the electron affinity of the substituent, while Bp-X has a twisted structure regardless of the type of substituent. In addition, the Δf values clearly show a linear correlation with the σ_p values for both electron-donating and -withdrawing groups. From the theoretical and experimental results, we show that Bp-$X^{\bullet-}$ substituted with an electron-donating and -withdrawing group at the *para* position has a slightly twisted structure, whereas Bp-$H^{\bullet-}$ has a planar geometry. The twisted structure of Bp-$X^{\bullet-}$ is due to the localization of the unpaired electron and negative charge on one benzene ring. Indeed, the theoretical calculations show that the unpaired electron and negative charge in Bp-$X^{\bullet-}$ substituted with an electron-donating group is located on the unsubstituted benzene ring, whereas that in Bp-$X^{\bullet-}$ substituted with an electron-withdrawing group is located on the substituted benzene ring. The experimental and theoretical results clearly reveal that the structure of Bp-$X^{\bullet-}$ is predominantly governed by the distribution of the unpaired electron and charge density between the two benzene rings, whereas in the ground state, the structure of Bp-H is governed by the steric interactions between the *ortho* atoms.

EXPERIMENTAL SECTION

Biphenyls with various substituents at the *para* position (Bp-X; X = −OH, $-OCH_3$, $-CH_3$, −H, $-CONH_2$, −COOH, and −CN) were purchased from Sigma-Aldrich and used without further purification.

Pulse Radiolysis. Pulse radiolysis experiments were performed using an electron pulse (27 MeV, 11 A, 8 ns, 0.8 kGy per pulse) generated by a linear accelerator at Osaka University.

TR^3 Spectroscopy. Bp-X's were dissolved in DMF, and the sample solutions were purged with argon gas during the TR^3 measurements. The Raman experiments were performed by passing the sample solution through a quartz capillary tube at a rate sufficient to ensure that each electron beam and laser pulse encountered a fresh sample volume. When accumulation was required for improving the signal-to-noise ratio, the sample was frequently replaced with a fresh sample. The TR^3 spectra for Bp-X during the pulse radiolysis were obtained by photoexcitation with a 416 nm laser pulse, which was generated by hydrogen Raman shifting of the third harmonic (355 nm) from a nanosecond Q-switched Nd:YAG laser (5 ns fwhm, Brilliant, Quantel; Les Ulis, France). The laser light for the Raman probe was synchronized with the electron pulse. The TR^3 spectra were collected using a polychromator (Acton, SP2500i; Trenton, NJ) equipped with a charge-coupled device (CCD) camera (Princeton Instruments, PI-MAX3; Trenton, NJ).

Theoretical Calculation. Optimized structures of Bp-X and Bp-$X^{\bullet-}$ were estimated using density functional theory (DFT) at the B3LYP/6-311+G(d,p) level. All theoretical calculations were carried out using the Gaussian 09 package.[34]

ASSOCIATED CONTENT

Supporting Information

Additional information as noted in the text. This material is available free of charge via the Internet at http://pubs.acs.org.

AUTHOR INFORMATION

Corresponding Authors

*Tel.: +81-6-6879-8495. Fax: +81-6-6879-8499. E-mail: jkchoi@ibs.re.kr.

*E-mail: majima@sanken.osaka-u.ac.jp.

Notes

The authors declare no competing financial interest.

DOI: 10.1021/jp511229t
J. Phys. Chem. A 2015, 119, 851−856

■ ACKNOWLEDGMENTS

We thank the members of the Research Laboratory for Quantum Beam Science of ISIR, Osaka University, for running the linear accelerator. This work has been partly supported by a Grant-in-Aid for Scientific Research (Projects 24550188, 25220806, and 25288035) from the Ministry of Education, Culture, Sports, Science and Technology (MEXT) of Japanese Government. J.C. thanks IBS-R004-G2 for support.

■ REFERENCES

(1) Zerbi, G.; Sandroni, S. Fundamental frequencies and molecular configuration of biphenyl—I. Re-analysis of its vibrational spectrum. *Spectrochim. Acta, Part A* **1968**, *24*, 483−510.
(2) Zerbi, G.; Sandroni, S. Fundamental frequencies and molecular configuration of biphenyl−—II Normal coordinates. *Spectrochim. Acta, Part A* **1968**, *24*, 511−528.
(3) Trotter, J. The crystal and molecular structure of biphenyl. *Acta Crystallogr.* **1961**, *14*, 1135−1140.
(4) Hargreaves, A.; Rizvi, S. H. The crystal and molecular structure of biphenyl. *Acta Crystallogr.* **1962**, *15*, 365−373.
(5) Schmid, E. D.; Brosa, B. Determination of conjugation and angle of twist in biphenyls by Raman intensity. *J. Chem. Phys.* **1972**, *56*, 6267−6268.
(6) Barrett, R. M.; Steele, D. Vibrational-spectra and dihedral angles of biphenyl and 4,4-dihalogenobiphenyls. *J. Mol. Struct.* **1972**, *11*, 105−125.
(7) Eaton, V. J.; Steele, D. Dihedral angle of biphenyl in solution and molecular force-field. *J. Chem. Soc., Faraday Trans. 2* **1973**, *69*, 1601−1608.
(8) Charbonneau, G. P.; Delugeard, Y. Structural transition in polyphenyls. III. Crystal structure of biphenyl at 110 K. *Acta Crystallogr.* **1976**, *B32*, 1420−1423.
(9) Monig, J.; Asmus, K. D.; Robertson, L. W.; Oesch, F. Polychlorinated biphenyl radical cations - a pulse-radiolysis investigation. *J. Chem. Soc., Perkin Trans. 2* **1986**, 891−896.
(10) Almenningen, A.; Bastiansen, O.; Gundersen, S.; Samdal, S. Structure and barrier to internal-rotation of biphenyl derivatives in the gaseous state. 6. On the molecular-structure and internal-rotation of 2,2′-bipyridine. *Acta Chem. Scand.* **1989**, *43*, 932−937.
(11) Furuya, K.; Torii, H.; Furukawa, Y.; Tasumi, M. Density functional study on the structures and vibrational spectra of the radical anion and cation of biphenyl. *J. Mol. Struct.* **1998**, *424*, 225−235.
(12) Grein, F. Twist angles and rotational energy barriers of biphenyl and substituted biphenyls. *J. Phys. Chem. A* **2002**, *106*, 3823−3827.
(13) Lapouge, C.; Buntinx, G.; Poizat, O. Resonance Raman spectra simulation of the biphenyl anion and cation radicals. *J. Mol. Struct.* **2003**, *651*, 747−757.
(14) Devlin, J. P.; Mckennis, J. S.; Thornton, C.; Moore, J. C. Vibrational-spectra of the benzene radical-anion and the dianion of biphenyl. *J. Phys. Chem.* **1982**, *86*, 2613−2616.
(15) Nakabayashi, T.; Kamo, S.; Sakuragi, H.; Nishi, N. Time-resolved Raman studies of photoionization of aromatic compounds in polar solvents: Picosecond relaxation dynamics of aromatic cation radicals. *J. Phys. Chem. A* **2001**, *105*, 8605−8614.
(16) Batonneau-Gener, I.; Moissette, A.; Bremard, C.; Buntinx, G. Time resolved resonance Raman, transient diffuse reflectance and kinetic studies of species generated by UV laser photolysis of biphenyl occluded within dehydrated Y-faujasite zeolites. *J. Photochem. Photobiol., A* **2008**, *195*, 156−166.
(17) Kato, C.; Hamaguchi, H. O.; Tasumi, M. Transient absorption and Raman-spectra of the S-1 state and the cation radical of biphenyl in solution. *Chem. Phys. Lett.* **1985**, *120*, 183−187.
(18) Buntinx, G.; Poizat, O. Triplet (T_1) state and radical cation resonance Raman investigation of biphenyl derivatives. *J. Chem. Phys.* **1989**, *91*, 2153−2162.
(19) Sasaki, Y.; Hamaguchi, H. O. Raman-spectra and structure of biphenyl isoatomers (the S_0, S_1, T_1 states and the cation and anion-radicals). *Spectrochim. Acta, Part A* **1994**, *50*, 1475−1485.
(20) Fujitsuka, M.; Majima, T. Recent approach in radiation chemistry toward material and biological science. *J. Phys. Chem. Lett.* **2011**, *2*, 2965−2971.
(21) Choi, J.; Fujitsuka, M.; Tojo, S.; Majima, T. Folding dynamics of cytochrome c using pulse radiolysis. *J. Am. Chem. Soc.* **2012**, *134*, 13430−13435.
(22) Fujitsuka, M.; Cho, D. W.; Tojo, S.; Choi, J.; Huang, H.-H.; Yang, J.-S.; Majima, T. Radical cation of star-shaped condensed oligofluorenes having isotruxene as a core: Importance of rigid planar structure on charge delocalization. *J. Phys. Chem. A* **2014**, *118*, 2307−2315.
(23) Choi, J.; Tojo, S.; Fujitsuka, M.; Majima, T. Dynamics in the heme geometry of myoglobin induced by the one-electron reduction. *Int. J. Radiat. Biol.* **2014**, *90*, 459−467.
(24) Saeki, A.; Kozawa, T.; Ohnishi, Y.; Tagawa, S. Reactivity between biphenyl and precursor of solvated electrons in tetrahydrofuran measured by picosecond pulse radiolysis in near-ultraviolet, visible, and infrared. *J. Phys. Chem. A* **2007**, *111*, 1229−1235.
(25) Das, S.; Kamat, P. V. Spectral characterization of the one-electron oxidation product of cis-bis(isothiocyanato)bis(4,4′-dicarboxylato-2,2′-bipyridyl) ruthenium(II) complex using pulse radiolysis. *J. Phys. Chem. B* **1998**, *102*, 8954−8957.
(26) Thomas, M. F.; Li, L. L.; Handley-Pendleton, J. M.; van der Lelie, D.; Dunn, J. J.; Wishart, J. F. Enzyme activity in dialkyl phosphate ionic liquids. *Bioresour. Technol.* **2011**, *102*, 11200−3.
(27) Dimitrijevic, N. M.; Bartels, D. M.; Jonah, C. D.; Takahashi, K.; Rajh, T. Radiolytically induced formation and optical absorption spectra of colloidal silver nanoparticles in supercritical ethane. *J. Phys. Chem. B* **2001**, *105*, 954−959.
(28) Grills, D. C.; Farrington, J. A.; Layne, B. H.; Lymar, S. V.; Mello, B. A.; Preses, J. M.; Wishart, J. F. Mechanism of the formation of a Mn-based CO_2 reduction catalyst revealed by pulse radiolysis with time-resolved infrared detection. *J. Am. Chem. Soc.* **2014**, *136*, 5563−5566.
(29) Choi, J.; Cho, D. W.; Tojo, S.; Fujitsuka, M.; Majima, T. Configurational changes of heme followed by cytochrome c folding reaction. *Mol. BioSyst.* **2015**, *11*, 218−222.
(30) Takahash, C.; Maeda, S. Raman-spectra of biphenyl negative-ion in tetrahydrofuran solution. *Chem. Phys. Lett.* **1974**, *24*, 584−588.
(31) Hammett, L. P. The effect of structure upon the reactions of organic compounds. Benzene derivatives. *J. Am. Chem. Soc.* **1937**, *59*, 96−103.
(32) Hansch, C.; Leo, A.; Taft, R. W. A survey of Hammett substituent constants and resonance and field parameters. *Chem. Rev.* **1991**, *91*, 165−195.
(33) Lewis, M.; Bagwill, C.; Hardebeck, L. K.; Wireduaah, S. The use of hammett constants to understand the non-covalent binding of aromatics. *Comput. Struct. Biotechnol. J.* **2012**, *1*, e201204004.
(34) Frisch, M. J.; Trucks, G. W.; Schlegel, H. B.; Scuseria, G. E.; Robb, M. A.; Cheeseman, J. R.; Scalmani, G.; Barone, V.; Mennucci, B.; Petersson, G. A.; et al. *Gaussian 09*; Gaussian, Inc.: Wallingford, CT, 2009.

DOI: 10.1021/jp511229t
J. Phys. Chem. A 2015, 119, 851−856